A linear recursive state of power estimation method based on fusion model of voltage and state of charge limitations.

LI, B., WANG, S., FERNANDEZ, C., YU, C., XIA, L. and FAN, Y.

2021

A linear recursive state of power estimation method based on fusion model of voltage and state of charge limitations

Bowen Li a, Shunli Wang a,*, Carlos Fernandez h, Chunmei Yu a, Lili Xia a, Yongcun Fan a

a School of Infonnation Engineering, Southwest University of Science and Technology, Mianyang 621010, China
b School of Phannacy and Life Sciences, Robert Gordon University, Aberdeen, AB10-7GJ, UK

ABSTRACT

As the main candidate of energy storage system for electric vehicles and hybrid electric vehicles, lithium-ion battery has attracted extensive attention. The working characteristics of the battery under dynamic stress stimulation are complex and changeable. To solve the problem of high-precision state of power estimation, a fusion model based on adaptive forgetting factor recursive least squares identification and voltage and charge state constraints was proposed, and a continuous discharge state of power analysis model for lithium-ion batte1ies was established. The adaptive forgetting factor recursive least square method based on battery model provides accurate and reliable online parameter identification feedback. The results show that the accuracy error of online parameter identification is less than 0.02V; the combination of the linear recursive algorithm of state of power analysis and the fusion model of voltage and current limit makes the power state estimation more reliable and accurate. The results show that when the battery is t=lOs, the peak discharge power error is less than SOW.

Keywords: lithium ion batteries; electric vehicle; state of power; fusion model; adaptive forgetting factor recursive least square algorithm; linear recursion algorithm

1. Introduction

Due to high energy density and high power, lithium-ion batteries have become a popular choice for energy storage systems for Electric Vehicles (EVs) and Hybrid Electric Vehicles (HEVs) [1-3]. The perfor-mance index of lithium-ion batteries can provide car owners with accurate information reference, which not only improves the product experience but also guarantees driving safety [4-6]. As the main observation system reflecting the performance and safety indicators of automobiles, the battery management system needs to provide accurate performance reference and reliable safety feedback for the two types of vehicles [7-9]. Nowadays, as the cruising range of new energy vehicles continues to increase, its application scenarios have undergone tremendous changes.

High range, high output power and high safety have become the main bottlenecks restricting the development of new energy vehicles [10-13]. State of Power (SOP) of lithium-ion battery can enrich various parameters of battery management system, provide reference to automobile power and guarantee for automobile driving safety [14-16]. The SOP of a lithium-ion battery is defined as the maximum available power that the battery can provide in the next time period, and it usually has a strong coupling relationship with the battery's current voltage, current and battery internal parameters [17]. Correspondingly, the specific maximum output or maximum input power of EVs and HEVs is reflected in the SOP [18-20]. According to the requirements of vehicles starting or accelerating control, the characteristics of battery output and input power are analyzed, and the battery energy management is greatly optimized.

Closely connected with the aforementioned content, because of the discretization of the build lithium-ion battery model to describe the condition of the experiment is indispensable [21,22]. There are three main types of battery models for performance characterization of lithium ion batteries: Electrochemical Model (EM), Equivalent Circuit Model (ECM) and Electrochemical Impedance Model (EIM) [23-25]. Zhang, X., et al. proposed a method for parameter identification of lithium-ion battery ECM considering electrochemical performance, and improved pseudo-two-dimensional (P2D) model is established based on partial differential equations (PDE) [26]. Yang, X., et al. fully considers the solid phase lithium ion diffusion equation, and based on the electrode average model of lithium ion batteries, the finite difference method is used to simplify the EM [27]. By analyzing the electro-chemical impedance spectroscopy of lithium ion batteries, the constant phase element (CPE) is introduced into the traditional time-domain circuit model, and the equivalent circuit model based on electrochemical impedance is constructed using fractional order theory [28]. The aforementioned work not only relies on a large amount of data but also has a high computational complexity.

The complexity and accuracy of the model need to be considered. The ECM conforms to the complexity and simplification of the model and can have high accuracy [29-32]. The precision of battery modeling usually depends on the detem1ination of model parameters, which depend on the measured data of the external characteristics of the battery [33-35]. However, due to environmental noise and measurement errors, it will lead to the estimation accuracy of model parameters. (i) consider the influence of voltage and current changes in working conditions: Wen, F.Z. proposed a method based on random response reconstruction to reconstruct the measured battery voltage data, and established the relationship between the battery voltage and current based on the second-order ECM [36]. (ii) the influence of environmental temperature change: Pang, H., L.J. Mou, and L. Guo proposed an enhanced ECM considering the effect of different ambient temperatures on the Open Circuit Voltage (OCV) of lithium ion batteries. The per-formance of lithium ion battery is slightly different from the ECM of different order.

Based on the foregoing work, the calculation of SOP often relies on other parameters to limit the feedback of its value [37-39]. It empha-sized that the battery characteristics change over time, the maximum available power for the battery is described [40-42]. Lei, Xu constructed a temperature-hysteresis fully coupled model, and analyzed the model parameters under different ambient temperatures, and realized the multi-state joint estimation of SOC and SOP [43]. Cheng, Ze proposed a combined constraint intelligent algorithm based on the results of SOC, battery voltage, and battery current to achieve high-precision charac-terization of operating conditions under the pulse discharge/charge test method [44]. Lin Peng proposed an improved current and time-based polarization voltage (NPV) model to achieve SOP prediction with an overall error of about 5% when t-second=l0s [45]. Although high-precision equivalent modeling can better characterize the battery status, the coupling effects berween various factors will inevitably bring interference. Not only is the computational burden large, but also re-quires huge experimental data support.

* Corresponding author.
E-mail address: wangshunli@swust.edu.com (S. Wang).

Therefore, for complex and unknown batteries, previous previous estimates are not conducive to practical applications. The influence of the internal parameters of the SOP algorithm has a great influence on the estimation result. The research analyzed the estimation accuracy of SOP under different constraints, and proposed an online parameter identification algorithm based on linear recursive fusion model to estimate SOP. The fusion model can correct the parameters with high precision according to the input conditions under complex working conditions, and can effectively avoid the low-precision fitting representation that occurs when the SOC of the battery is too low. The fusion model first uses the improved adaptive forgetting factor recursive least square method to analyze the input data, and realizes the reliable online analysis of the parameters. On this basis, a fusion model based on voltage and SOC constraints is constructed, and SOC is used as a scale for quantitative analysis to realize online high-precision SOP simulation output of complex models.

2. Mathematical analysis

2.1. Lithium ion battery modeling

The accurate characterization of the state of lithium-ion batteries cannot be achieved without reliable and processable battery models. The proposed study is based on the multi-parameter fusion algorithm, and the use of high-order models will produce a large number of high-order matrices, which makes the calculation complex and increases the calculation time. Therefore, considering the accuracy and complexity of the lithium-ion battery model, the Thevenin model was selected to demonstrate the operating characteristics, as shown in Fig.I, and the online feedback operating characteristics were used to describe the variation characteristics of the battery voltage.

The ECM shown in Fig.I is mainly divided into four parts: (i) Battery terminal voltage Uocv (SOC) is the battery characteristic voltage ob-tained according to the identification of SOC value; (ii) Ohmic resistance Ro under the equivalent characterization of the battery; (iii) RC circuit network characterizing the polarization effect of the battery, including the polarization resistor Rp and the polarization capacitor Cp; The OCV UL that characterizes the load voltage under battery load conditions; Up represents voltage under polarization effect; Ut stands for ohmic effect and polarization effect voltage and; IL is the discharge current of a lithium battery.

Thus, the model of this circuit can be represented as

$$\begin{cases} \chi_k = A_{k-1}\chi_{k-1} + B_{k-1} + I_{L,k-1} \\ UT = f(\chi_k, I_{L,k}) \end{cases} \tag{1}$$

Where

$$\begin{aligned} &\chi_k = \left[U_{p,k} SOC_k\right]^T \\ &A_{k-1} = \begin{bmatrix} \varepsilon_{k-1} & 0 \\ 0 & 1 \end{bmatrix} \\ &B_{k-1} = \left[R_{p,k-1}(1-\varepsilon_{k-1}) \quad \frac{t}{3600 Q_c}\right]^T \\ &\varepsilon_{k-1} = e^{\frac{t}{R_{p,k-1} C_{p,k-1}}} \\ &f(\chi_k, I_{L,k}) = U_{ocv(SOC),k} + R_{o,k} I_{L,k} + U_{p,k} \end{aligned} \tag{2}$$

Among them, k represents the time at each moment; t represents the sampling time; Qc represents the battery capacity. The coupling relationship formed by the above parameters represents the internal state of the battery in various complex environments.

2.2. Online parameter identification based on Adaptive Forgetting Factor Least Square Method

The parameter characterization of the lithium-ion battery model is based on the SOC-OCV curve. Accurate SOC-OCV curve is an essential part of the parameter identification process. But in the long-term application of the entire system, the ability to identify battery parame-ters is full of obstacles. This paper adopts the adaptive recursive forgetting factor least square method (AFFRLS) to analyze the fluctuation data in the time domain, and continuously correct the factors according to the variance of the error variance to obtain the optimal internal factor coupling relationship, and realize the real-time estimation of battery parameters .

Parameter identification is often a further coupled analysis of the intrinsic functional relationship between voltage and current. Data preprocessing is often required at the input, that is, the voltage error is checked first, which introduces a new amount of error to a large extent. The flow chart of the AFFRLS algorithm for lithium-ion batteries with pre-data processing is shown in Fig. 2.

Among them, X(t) represents the input of the battery's working state, including current, voltage, and the SOC-OCV curve verified by HPPC in the previous period; Y(t) represents the parameters under online identification, including ohmic resistance, polarization capacitance, and polarization resistance,etc; e(t) represents the error; the part indicated by the dotted line represents the initial value introduction. The ability to accurately analyze the working characteristics of lithium-ion batteries depends on the accurate analysis of the model and the reliable representation of the model state equation. According to Fig. 2, the least-squares representation transformation of the equivalent circuit model is described in detail. The specific process of transforming the equivalent circuit model of lithium-ion battery into the least square method is shown in Fig. 3.

Among them, S1 represents the lithium-ion battery model currently analyzed; S2 describes the characteristics of discrete batteries, which is introduced a frequency domain factor to analyze Equation 2; S3 repre-sents the transfer function relationship berween voltage and current, which is the analysis of the internal relationship berween voltage and current; S4 represents the analysis of the bilinear changes introduced by the s domain; S5 describes the internal connection between the pa-rameters in the z-domain transfer function, and uses S4 and S3 to aggregate and split variables to obtain the coupling representation of voltage and current and their internal factors; S6 represents the param-eter representation form. By building the framework of the functions shown in Fig. 3, the demonstrative representation shown in Equation 3 can be obtained.

$$\begin{cases} E_2 = \theta_{1,1}E_1 + \theta_{2,1}I_{L,2} + \theta_{3,1}I_{L,1} + e_1(k) \\ E_3 = \theta_{1,2}E_2 + \theta_{2,2}I_{L,3} + \theta_{3,2}I_{L,2} + e_2(k) \\ \vdots\vdots\vdots. \\ E_k = \theta_{1,k-1}E_{k-1} + \theta_{2,k-1}I_{L,k} + \theta_{3,k-1}I_{L,k-1} + e_{k-1}(k) \end{cases} \tag{3}$$

Where, E_k represents the difference between the actual operating condition electric UL and the simulated voltage Uocv (SOC). Under the complex working conditions of lithium-ion batteries, the internal rela-tionship between SOC and OCV is difficult to obtain. The acquisition of the simulated voltage often relies on priori data analysis. On the one hand, it brings a lot of early calculations, on the other hand, it introduces the systematic error of curve simulation. Through the expansion of the matrix, E_k in Equation 3 is analyzed to separate $UL,_k$ and Uocv,k, and the equation is rewritten as shown in Equation 4.

$$\begin{cases} U_{L,2} = U_{\text{ocv},2} + \theta_{1,1}U_{\text{ocv},1} + \theta_{1,1}U_{L,1} + \theta_{2,1}I_{L,2} + \theta_{3,1}I_{L,1} + e_1(k) \\ U_{L,3} = U_{\text{ocv},3} + \theta_{1,2}U_{\text{ocv},2} + \theta_{1,2}U_{L,2} + \theta_{2,2}I_{L,3} + \theta_{3,2}I_{L,2} + e_2(k) \\ \vdots\vdots\vdots\vdots \\ U_{L,k} = U_{\text{ocv},k} + \theta_{1,k-1}U_{\text{ocv},k-1} + \theta_{1,k-1}U_{L,k-1} + \theta_{2,k-1}I_{L,k} + \theta_{3,k-1}I_{L,k-1} + e_{k-1}(k) \end{cases} \tag{4}$$

Simplify the analysis of the matrix by introducing new variables (the formula only represents the equivalent expression without error interference) as shown in Equation 5. Uocv becomes a function variable related to the initial value and algorithm modification.

$$\begin{cases} U_{L,k} = \varphi_k\sigma_k^T + e_{k-1} \\ \varphi_k = \left[1\, U_{L,k-1}\, I_{L,k}\, I_{L,k-1}\right] \\ \sigma_k = \left[U_{\text{ocv},k} + \theta_{1,k-1}U_{\text{ocv},k-1}\, \theta_{1,k-1}\, \theta_{2,k-1}\, \theta_{3,k-1}\right] = \left[\sigma_{1,k}\sigma_{2,k}\sigma_{3,k}\sigma_{4,k}\right] \end{cases} \tag{5}$$

Wherein, φ_k is the observation vector, $б_k$ is the parameter vector to be estimated. Taking voltage and current as input parameters, using the characteristics of least square method, combined with the above circuit model analysis method, real-time variation of battery parameters can be obtained. The flow chart of the improved AFFRLS algorithm is shown in Fig. 4.

As shown in Fig. 4, the algorithm theme consists of 6 parts, including data input, algorithm processing, parameter output and so on. The following will further elaborate on the algorithm flow.

(i) Data input: By analyzing the working characteristics of lithium-ion battery current, voltage, it is used as algorithm real-time data input.

(ii) Transformation equation: Transform the equation for known factors (voltage and current), and construct a matrix equation for continuous response; In consideration of the influence of noise, a matrix e(k) is introduced to characterize this interference; The simplified matrix is expressed as $U_{L,k=}\varphi_k б_{k+}e_{k,}$

(iii) Metric discrete function: According to the relationship between the system input and the system output, the n-dimensional rep-resentation of the matrix can be obtained after changing and processing the matrix coefficients; The LS method is to optimize data under fluctuating conditions; The parameter correction at each moment should be based on the reliable last-minute correction value and the changing conditions; Combined with the foregoing, the modified parameter correction relation can be obtained as $б_k=((\varphi_k^T\varphi_k)^{-1}\varphi_k^T U_{L,k})$.

(iv) Forecast equation update: The prediction and update can enhance the optimization effect at the following moments, so as to avoid the situation that the gain(K) and matrix variance(P) of the algorithm become smaller and smaller due to the increase of iteration times; among them, according to a large number of experiments, the forgetting factor is usually set at 0.96 ~ 1.

(v) Forgetting factor update: AFFRLS obtains an algorithm tracking effect more in line with the actual changes of the working conditions through the continuous modification of the forgetting factor; Among them, λ_{min} is the minimum value of forgetting factor;limit indicates that the reference object is restricted so that its maximum value does not exceed l; g is the sensitivity coeffi-cient that can be chosen to be any value between O to 1, indicating the sensitivity of the forgetting factor to errors; e_k is the error at time k;e_{base} is the allowed error reference; round(n) represents the integer closest to n.

(vi) Real-time parameter output: The output of the algorithm is calculated by the combination of the AFFRLS algorithm correction factor and the least square form of the equivalent circuit model.

According to the above, the improved AFFRLS can track and analyze the voltage and working current inside the battery in real time, analyze the changes of battery characteristic parameters, and provide a reliable parameter tracking curve to estimate the state of the lithium-ion battery. Compared with AFFRLS with data preprocessing, the theme of this algorithm reduces the process related to preliminary experimental analysis and data fitting, and effectively improves the adaptability and operability of the algorithm.

2.3. State of Power estimation under fusion algorithm

EVs often use batteries for group applications. When the SOC of the battery pack is extremely low, the problem of inconsistency between the cells will occur. Compared with other cells, the voltage of individual cells is too high or too low. Estimating the voltage will inevitably lead to incorrect estimates. In addition, when the battery is in a charged state, problems such as overcharging will occur due to battery aging and only relying on voltage to estimate battery power.

Accurate estimation of the SOP of the lithium battery can achieve the best power distribution, avoid overcharge and overdischarge of the battery, and extend the service life of the lithium battery.The operation of an EVs usually requires a peak current of several seconds or tens of seconds to operate continuously. Therefore, the analysis of continuous time vehicle operation is conducive to a wide range of practical appli-cations. As shown in Fig. 5, considering the operating characteristics of the battery, a fusion estimation model under the limits of voltage and SOC is proposed to estimate SOP.

The characterization of the status of lithium-ion batteries is inseparable from accurate analysis of battery parameters. As shown in Fig. 5, the improved AFFRLS can provide high-precision voltage simulation. By combining the voltage limit, it can simulate the non-linear state of the battery, and the fusion model estimation of the SOC limit is introduced, which greatly improves the safety and reliability of the system.Among them, the real-time estimation of SOC is carried out through the UKF algorithm. For complex operating conditions, it is difficult to estimate the internal SOC state. UKF has better convergence against initial errors, better robustness, and less computational burden, which is conducive to real-time tracking and analysis of working conditions.For the above related processes, the voltage limit and SOC limit and their fusion analysis are further explained.Assuming that the peak current in the selected stage is constant within the sampling time KT, Equation 6 can be obtained.

$$\chi_{k+K_T} = A_k^{K_T} + \left(\sum_{n=1}^{K_T} A_k^{n-1} B_k\right) I_{L,k} \tag{6}$$

Among them, the polarization voltage of continuous response can be described as

$$\begin{cases} U_{p,k+K_T} = U_{p,k} e^{-\frac{K_T}{t_p}} + \left(1 - e^{-\frac{K_T}{t_p}}\right) R_{p,k} I_{L,k+K_T} \\ t_{p,k} = R_{p,k} \times C_{p,k} \end{cases} \tag{7}$$

Where K_T represents the sampling time width. Using Taylor's formula to expand OCV(SOC) at k sampling time, and ignoring multiple high-order terms, Equation 8 can be obtained to describe the internal relationship between battery OCV.

$$OCV(SOC_{k+K_T}) = OCV(SOC_k) - \frac{\eta K_T}{Q_c} \frac{\partial OCV(SOC_k)}{\partial SOC_k} I_{L,k+K_T} \tag{8}$$

The terminal voltage is one of the main factors affecting the peak current of battery discharge. Combined with Equation 7 and Equation 8, the working state of the battery under the battery duration is analyzed, and the current expression formula of terminal voltage is obtained as shown in Equation 9.

$$\begin{aligned} U_{L,k+K_T} = {} & OCV(SOC_k) - U_{p,k} e^{-\frac{K_T}{t_{p,k}}} \\ & - I_{L,k+K_T} \left[\frac{\eta K_T}{Q_c} \frac{\partial OCV(SOC_k)}{\partial SOC_k} + R_{o,k} + \left(1 - e^{-\frac{K_T}{t_{p,k}}}\right) R_{p,k}\right] \end{aligned} \tag{9}$$

However, the voltage design limit of lithium battery is certain in actual operation. The operating voltage at any time shall meet the limitation of terminal voltage (Vmax = 4.2V, Vmin = 2.SV). Therefore, the continuous peak current of battery charging and discharging under voltage limita-tion is expressed as Equation 10.

$$\begin{aligned} & \frac{v_{\min} - U_{ocv(SOC),k+K_T} + \varepsilon_{k+K_T}{}^{K_T} U_{p,k+K_T}}{\frac{\eta K_T t}{Q_{c,k}} \times \left.\frac{\partial U_{ocv(SOC)}}{SoC}\right|_{SoC=SoC_{k+K_T}} + R_{o,k+K_T} + R_{p,k+K_T}(1-\varepsilon_{k+K_T}) \sum_{n=1}^{K_T} \varepsilon_{k+K_T}{}^{n-1}} \\ & \frac{v_{\max} - U_{ocv(SOC),k+K_T} + \varepsilon_{k+K_T}{}^{K_T} U_{p,k+K_T}}{\frac{\eta K_T t}{Q_{c,k}} \times \left.\frac{\partial U_{ocv(SOC)}}{SoC}\right|_{SoC=SoC_{k+K_T}} + R_{o,k+K_T} + R_{p,k+K_T}(1-\varepsilon_{k+K_T}) \sum_{n=1}^{K_T} \varepsilon_{k+K_T}{}^{n-1}} \end{aligned} \tag{10}$$

Among them,$I^V_{dis,k+KT}$ is the characterization of the battery discharge current under the voltage limit; $I^V_{cha,k+KT}$ is the battery characterization of the charge current under the voltage limit.

In addition, the SOC of the battery reflects the safety and reliability of the battery. In order to ensure the safe operation of the electric vehicle power battery pack, the SOC of the lithium battery at any time needs to meet certain restrictions, that is, $SOC_{min} \leq SOC_k \leq SOC_{max}$. Then, under the limitation of SOC at the current moment, the continuous peak discharge current and continuous peak charging current in the future time period can be expressed as Equation 11 respectively.

$$\begin{cases} I^{SOC}_{dis,k+K_T} = \dfrac{SOC_k - SOC_{\min}}{\eta K_T / Q_c} \\ I^{SOC}_{cha,k+K_T} = \dfrac{SOC_k - SOC_{\max}}{\eta K_T / Q_c} \end{cases} \tag{11}$$

Among them, SOCmin represents the minimum SOC value that the battery can operate; SOCmax represents the maximum SOC value that the battery can operate. Combining the aforementioned two constraints and considering the design constraints of the battery itself, the peak current expression of the multiple constraints under the hybrid model can be obtained as shown in Equation 12.and considering the design constraints of the battery itself, the peak current expression of the multiple constraints under the hybrid model can be obtained as shown in Equation 12.

$$\begin{cases} I_{dis,k+K_T} = min\left\{I_{dis}, I^{SOC}_{dis,k+K_T}, I^{V}_{dis,k+K_T}\right\} I_{cha,k+K_T} = max\left\{I_{cha}, I^{SOC}_{cha,k+K_T}, I^{V}_{cha,k+K_T}\right\} \end{cases} \tag{12}$$

Wherein, Idis is the calibrated maximum discharge current of the battery; Icha is the calibrated maximum charging current of the battery. Obviously, the SOP prediction of the lithium ion battery at this time can be expressed by Equation 13.

$$\begin{cases} P_{dis,k+K_T} = U_{L,k+K_T}\left(I_{dis,k+K_T}\right) \times I_{dis,k+K_T} \\ P_{cha,k+K_T} = U_{L,k+K_T}\left(I_{cha,k+K_T}\right) \times I_{cha,k+K_T} \end{cases} \tag{13}$$

Among them, $P_{dis,k+KT}$ represents the battery discharge SOP under the voltage limit discharge; $P_{cha,k+KT}$ represents the battery discharge SOP under the voltage limit charge. By constructing the estimation system of peak output power under different durations, the battery characteristics under different states are analyzed, so as to provide reliable data reference for users.

3. Experimental analysis

3.1. Test platform construction and data analysis

The operation condition of the lithium ion battery needs to deliver reliable experimental testing process, and rely on the high precision testing equipment. The instruments used in this test are power battery high-power charge-discharge tester (CT-4016-5V100A-TFA), three-layer independent temperature control test box and other supporting experimental equipment (BT-331C). The experimental data test flow of the research object (lithium ion battery) is shown in Fig. 6.

The continuous response of the lithium-ion battery changes the state of the battery, thus changing the estimation of the battery peak. In this paper, discharge conditions with different durations were constructed, as shown in Fig. 7. By demonstrating the discharge state of lithium ion battery under different continuous excitation, a comparative analysis of discharge experiments under different conditions was constructed. It is worth mentioning that the lithium-ion battery with a capacity of 74.28Ah was used in the experiment and the experiment was carried out in a temperature control box set at 25 ℃.

Among them, Fig. 7 (a) demonstrates the HPPC pulse workflow to describe the different discharge conditions of the battery; Fig. 7 (b) demonstrates the BBDST pulse workflow, used to describe the power output conditions of the car in different states; Fig.7(c-e) demonstrates the current state of BBDST under different continuous peak discharges. Furthermore, Pt is the power discharge time, which changes the continuous excitation duration; VM_IM represents the current and voltage cut-off judgment.

When testing a lithium-ion battery in a constant power state (ie, BBDST working state), as the voltage decreases, the battery cannot maintain power output, which will cause the battery's operating current to fluctuate significantly. When the battery can provide sufficient voltage, it can capture the above-mentioned current change characteristics. However, when the battery is in trickle charge or discharge, the voltage change is not obvious for a short time, and a single factor is difficult to track and correct, which will cause system estimation errors.

3.2. Online parameter identification under continuous pulse conditions

In order to verify the reliability of the improved AFFRLS algorithm under complex working conditions, a quantitative analysis of AFFRLS with predata processing, improved AFFRLS and improved FRLS was constructed. Select the operating condition data shown in Fig. 7 (d) for comparative analysis, and the voltage simulation error and its partial amplification error diagram are shown in Fig. 8.

Among them, S1 represents the actual working condition voltage; S2 represents the voltage simulated by the improved AFFRLS algorithm; S3 represents the non-adaptive improved FRLS algorithm simulation voltage; S4 represents the AFFRLS algorithm simulation voltage with predata processing. It can be seen from Figu. 8(b) that S2 has the best robustness for the discharge part under complex working conditions, and the effect of S3 is better than that of S4; S4 only has a better effect on part of the charging section. Taking the entire BBDST experiment as the research object, the performance indicators of the three algorithms are shown in Table 1.

The regression characteristic index of the algorithm reflects the on-line identification accuracy of the algoritluu. It can be seen from the table that the improved AFFRLS algorithm that separates and analyzes the matrix has higher accuracy and can reflect the parameter identification performance requirements of lithium-ion batteries under complex conditions.

It is worth mentioning that with the increase of the duration of peak power output, the full discharge time of the battery will decrease sharply. Therefore, the time coordinate axis scale is inconsistent for different duration analysis. The improved AFFRLS algorithm is intro-duced to identify and analyze the working characteristics of battery continuous excitation as shown in Fig. 7 (c-e), and tl1e voltage error is shown in Fig. 9.

As shown in Fig. 9, the actual working voltage output of BBDST and the voltage simulation error under the online parameters of the lithium-ion battery were analyzed under the peak output of 10s, 30s and 60s. Where, U represents the acquisition voltage under real working conditions, and Uerr represents the voltage error under online parameters. As can be seen from the figure, the absolute value error of online simulation is kept within 0.02V for a long time. When the discharge of the battery can not meet the stable power output, the voltage error fluctuates under the on-line identification.

3.3. Working condition demonstration effect

The parameter identification accuracy of the online identification system greatly affects the status analysis of the lithium-ion battery. According to the common analysis of different working conditions, the variables based on sac are selected for curve fitting characterization. On the one hand, accurate SOC can provide high-precision simulation representation. On the other hand, SOC can provide correction for the sac under the fusion model. SOC estimation curve based on BBDST working condition of different duration, as shown in Fig. 10.

As shown in Fig. 10, Serr represents the error between the real value and the simulated value. The actual simulation estimation error of BBDST under three different sustained peak times is less than 1.5%. The power state of a litl1ium-ion battery is mainly related to me battery voltage, current and its internal state parameters. This study mainly analyzes the discharge-based experiment. The length of the continuous discharge time will cause a large change in the voltage, that is, the state of the lithium-ion battery under the excitation of different durations will change greatly. The relationship is analyzed by constructing HPPC ex-periments with three duration excitations of 10s, 30s and 60s, as shown in Fig. ll.

Among them, Fig. ll shows the P-SOC fitting curve under different durations, and the P-SOC polynomial expression is shown in Equation 14. Obviously, the power change under the HPPC test is relatively similar to the voltage change trend.

The estimation error of SOP mainly comes from internal parameters and characteristics of working conditions. The operating characteristics of EVs and HEVs have obvious changes under different working condi-tions. By analyzing the online identification of the same battery under the excitation of different continuous peak discharges, a battery peak state estimation system under the compound model is constructed. By combining the correlation between the various influencing factors, draw the SOP estimation curve and error curve of the lithium-ion battery, as shown in Fig. 12.

As shown in Fig. 12, US represents the power estimation under tl1e composite model of the lithium-ion battery, and the peak current is introduced to limit; U represents the estimated state of the lithium-ion battery under tl1e voltage limit; Act represents the reference state ob-tained through the HPPC test; Uerr Represents the power error under the voltage limit; USerr represents the power error under the composite model. As shown in Fig. 12 (a), the composite model can provide front-end power optimization with an overall error of less than l0OW when discharging at a sustained peak for a short time. As shown in Fig. 12 (b) and (c), with the increase of discharge time, the peak power in the latter half fluctuates greatly. The composite mode performance is sufficient to provide better back-end optimization capability, and the overall error remains within 250W.

The influence of different duration excitations under complex con-ditions will increase with the increase of the length of the time excita-tion. Analyzing the estimation error between each impact factor can help analyze the inherent problems of the algorithm. The evaluation of the algorimm's overall identification parameters is shown in Table 2.

As can be seen from me table, as tl1e excitation time goes by, the estimated errors of its voltage and peak power show a slow upward trend. The fusion algorithm has a strong tracking effect for short-term impulse excitation, and long-term excitation will receive more inter-ference. Effective estimation of balanced time pulses can provide higher power state tracking.

4. Conclusions

The proposed study creatively proposes a recursive adaptive LS method with forgetting factor and combines a fusion model under voltage and sac constraints to estimate SOP. In this paper, me voltage effect is characterized by the Thevenin model of the online OCV-SOC curve, and the battery characteristics are comprehensively analyzed. And combined with BBDST condition experiment to achieve high precision analysis. Under the condition of continuous change, the voltage error of on-line parameter identification is 0.02V. When the battery is at t=10s, the peak discharge power error is less than 80W; when the bat-tery is at t=60s, the peak discharge power error is less than 250W.

Author statement

The dissertation submitted is the research result of my independent research under the guidance of my supervisor. Except for the content specially marked and quoted in the article, this paper does not contain any other individual or collective works that have been published or written.

Declaration of Competing Interest

We declare that we have no financial and personal relationships with other people or organizations that can inappropriately influence our work, there is no professional or other personal interest of any nature or kind in any product, service and/or company that could be construed as influencing the position presented in, or the review of, the manuscript entitled "A linear recursive state of power estimation method based on fusion model of voltage and state of charge limitations".

Acknowledgments

The work was supported by the National Natural Science Foundation of China (No. 61801407).

Reference

[1] I.D. Campbell, et al., Optimising lithium-ion cell design for plug-in hybrid and battery electric vehicles, Journal of Energy Storage 22 (2019) 228–238.
[2] J. Kleiner, et al., Thermal Modelling of a Prismatic Lithium-Ion Cell in a Battery Electric Vehicle Environment: Influences of the Experimental Validation Setup, Energies 13 (1) (2020).
[3] N. Rizoug, et al., Development of new improved energy management strategies for electric vehicle battery/supercapacitor hybrid energy storage system, Energy Efficiency 11 (4) (2018) 823–843.
[4] J.T. Zhao, Z.H. Rao, Y.M. Li, Thermal performance of mini-channel liquid cooled cylinder based battery thermal management for cylindrical lithium-ion power battery (vol 103, pg 157, 2015), Energy Conversion and Management 155 (2018), 346-346.
[5] H.Q. Liu, E. Chika, J.Y. Zhao, Investigation into the effectiveness of nanofluids on the mini-channel thermal management for high power lithium ion battery, Applied Thermal Engineering 142 (2018) 511–523.
[6] J.W. Chen, et al., Effects of different phase change material thermal management strategies on the cooling performance of the power lithium ion batteries: A review, Journal of Power Sources (2019) 442.
[7] Y.X. Lai, et al., A compact and lightweight liquid-cooled thermal management solution for cylindrical lithium-ion power battery pack, International Journal of Heat and Mass Transfer (2019) 144.
[8] D. Kang, et al., Internal thermal network model-based inner temperature distribution of high-power lithium-ion battery packs with different shapes for thermal management, Journal of Energy Storage (2020) 27.
[9] J.Z. Ren, New energy vehicle in China for sustainable development: Analysis of success factors and strategic implications, Transportation Research Part D-Transport And Environment 59 (2018) 268–288.
[10] J.H. Lu, et al., Online Estimation of State of Power for Lithium-Ion Batteries in Electric Vehicles Using Genetic Algorithm, Ieee Access 6 (2018) 20868–20880.
[11] M.J. Esfandyari, et al., A new approach to consider the influence of aging state on Lithium-ion battery state of power estimation for hybrid electric vehicle, Energy 176 (2019) 505-520.
[12] A. Farmann, D.U. Sauer, Comparative study of reduced order equivalent circuit models for on-board state-of-available-power prediction of lithium-ion batteries in electric vehicles, Applied Energy 225 (2018) 1102-1122.
[13] X. Feng, B. Huang, Y.Y. Li, R&D investment in new energy vehicles with purchase subsidy based on technology adoption life cycle and customers' choice behaviour, let Intelligent Transport Systems 14 (11) (2020) 1371-1377.
[14] D. Liang, et al., An Efficient Ant Colony System Approach for New Energy Vehicle Dispatch Problem, Ieee Transactions on Intelligent Transportation Systems 21 (11) (2020) 4784-4797.
[15] Z.M. Wu, et al., Optimal mixed charging schemes for traffic congestion management with subsidy to new energy vehicle users, International Transactions In Operational Research (2020).
[16] H.M. Zhang, et al., Echelon utilization of waste power batteries in new energy vehicles: Review of Chinese policies, Energy (2020) 206.
[17] A.J. Wei, et al., A facile one-step solid-state synthesis of a Li4Ti5012/graphene composite as an anode material for high-power lithium-ion batteries, Solid State Jonics 329 (2019) 110--118.
[18] Y.B. Rao, New energy vehicles and sustainability of energy development: Construction and application of the Multi-Level Perspective framework in China. Sustainable Computing-Informatics & Systems, 2020, p. 27.
[19] F.S. Meng, X.Y. Jin, Evaluation of the Development Capability of the New Energy Vehicle Industry: An Empirical Study from China,
[20] K.D. Chen, et al., Synergistic Impacts of China's Subsidy Policy and New Energy Vehicle Credit Regulation on the Technological Development of Battery Electric Vehicles, in: Energies, 11, 2018.
[21] X. Lai, et al., Co-estimation of state of charge and state of power for lithium-ion batteries based on fractional variable-order model, Journal Of Cleaner Production (2020) 255.
[22] P. Lin, et al., Battery voltage and state of power prediction based on an improved novel polarization voltage model, Energy Reports 6 (2020) 2299-2308.
[23] P. Lin, et al., Novel Polarization Voltage Model: Accurate Voltage and State of Power Prediction, 8, Ieee Access, 2020, pp. 92039-92049.
[24] X. Liu, et al., An Improved State of Charge and State of Power Estimation Method Based on Genetic Particle Filter for Lithium-ion Batteries, Energies 13 (2) (2020).
[25] X. Tang, et al., Model migration based battery power capability evaluation considering uncertainties of temperature and aging, Journal Of Power Sources (2019) 440.
[26] X. Zhang, et al., A novel method for identification of lithium-ion battery equivalent circuit model parameters considering electrochemical properties, Journal Of Power Sources 345 (2017) 21-29.
[27] X. Yang, et al., Parameter Identification of Electrochemical Model for Vehicular Lithium-Ion Battery Based on Particle Swarm Optimization, in: Energies, 10, 2017.
[28] N. Chen, et al., Estimating the State-of-Charge of Lithium-Ion Battery Using an H-Infinity Observer Based on Electrochemical Impedance Model, 8, Ieee Access, 2020, pp. 26872-26884.
[29] X.P. Tang, et al., Load-responsive model switching estimation for state of charge of lithium-ion batteries, Applied Energy 238 (2019) 423--434.
[30] H. Khalifa, et al., Structurally Folded Curvature Surface Models of Geodes/Agate Rosettes (Cathode/Anode) as Vehicle/Truck Storage for High Energy Density Lithium-Ion Batteries, Batteries & Supercaps 3 (1) (2020) 76---92.
[31] S.L. Wang, et al., A novel safety assurance method based on the compound equivalent modeling and iterate reduce particle-adaptive Kalman filtering for the unmanned aerial vehicle lithium ion batteries, Energy Science & Engineering 8 (5) (2020) 1484-1500.
[32] Z. Cheng, et al., Power prediction method of lithium-ion battery for unmanned vehicles based on combined constraint intelligence algorithm, Cluster Computing-the Journal Of Networks Software Tools And Applications 22 (2019). S8553-S8560.
[33] W. Zhou, et al., A novel interval-based approach for quantifying practical parameter identifiability of a lithium-ion battery model, International Journal of Energy Research 44 (5) (2020) 3558--3573.
[34] F. Roder, V. Laue, U. Krewer, Model Based Multiscale Analysis of Film Formation in Lithium-Jon Batteries, Batteries & Supercaps 2 (3) (2019) 248-265.
[35] X. Lei, et al., A Novel Temperature-Hysteresis Model for Power Battery of Electric Vehicles with an Adaptive Joint Estimator on State of Charge and Power, Energies 12 (19) (2019).
[36] F.Z. Wen, et al., High-Accuracy Parameter Identification Method for Equivalent-Circuit Models of Lithium-Ion Batteries Based on the Stochastic Theory Response Reconstruction, Electronics 8 (8) (2019).
[37] H. Pang, L.J. Mou, L. Guo, Parameter identification and state-of-charge estimation approach for enhanced lithium-ion battery equivalent circuit model considering influence of ambient temperatures, Chinese Physics B (10) (2019) 28.
[38] J. Jiang, et al., Butler-Volmer equation-based model and its implementation on state of power prediction of high-power lithium titanate batteries considering temperature effects, Energy 117 (2016) 58-72.
[39] J. Lu, et al., Online Estimation of State of Power for Lithium-Ion Batteries in Electric Vehicles Using Genetic Algorithm, Ieee Access 6 (2018) 20868-20880.
[40] S.L. Wang, et al., An integrated online adaptive state of charge estimation approach of high-power lithium-ion battery packs, Transactions Of the Institute Of Measurement And Control 40 (6) (2018) 1892-1910.
[41] C. Wei, M. Benosman, T. Kim, Online Parameter Identification for State of Power Prediction of Lithium-ion Batteries in Electric Vehicles Using Extremum Seeking, International Journal Of Control Automation And Systems 17 (11) (2019) 2906---2916.
[42] X. Tang, et al., Long-Term Battery Voltage, Power, and Surface Temperature Prediction Using a Model-Based Extreme Leaming Machine, Energies 11 (1) (2018).
[43] X. Lei, et al., A Novel Temperature-Hysteresis Model for Power Battery of Electric Vehicles with an Adaptive Joint Estimator on State of Charge and Power, Energies 12 (19) (2019) 24.
[44] Z. Cheng, et al., Power prediction method of lithium-ion battery for urunanned vehicles based on combined constraint intelligence algorithm, Cluster Computing-the Journal Of Networks Software Tools And Applications 22 (2019). S8553- S8560.
[45] P. Lin, et al., Battery voltage and state of power prediction based on an improved novel polarization voltage model, Energy Reports 6 (2020) 2299-2308.

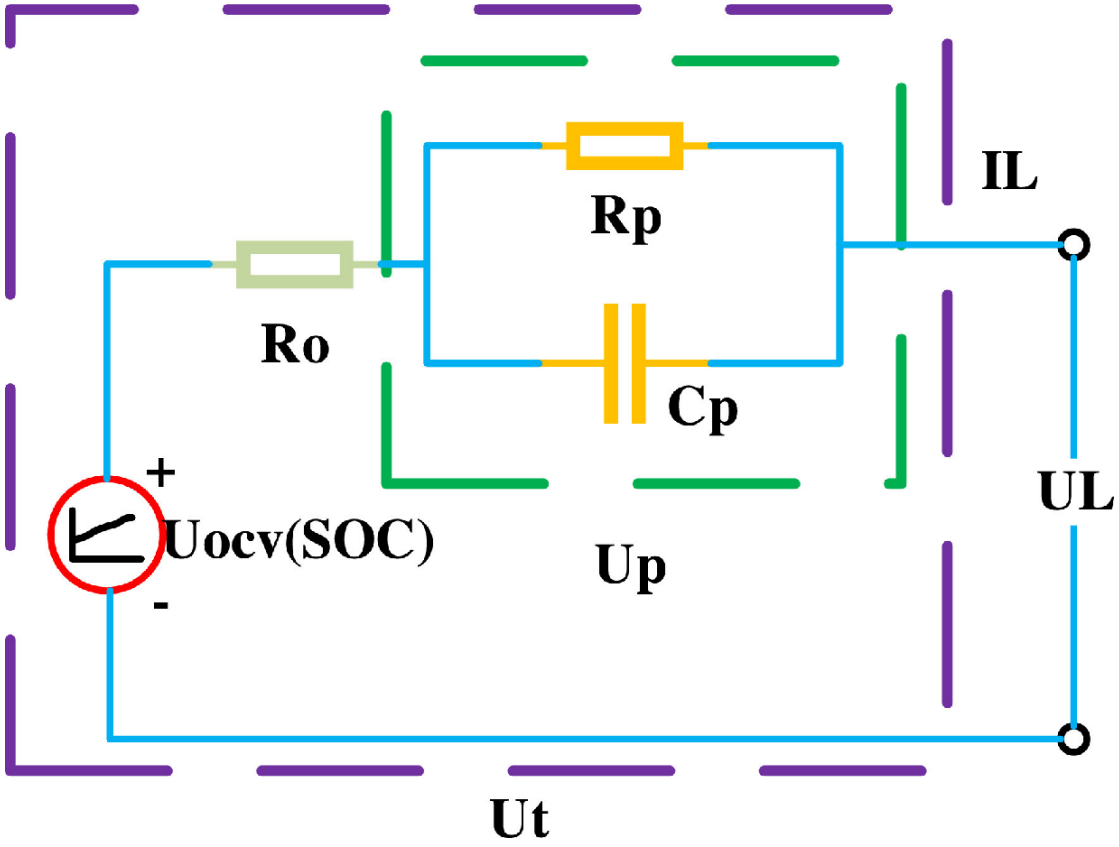

Fig. 1. The Thevenin equivalent circuit model

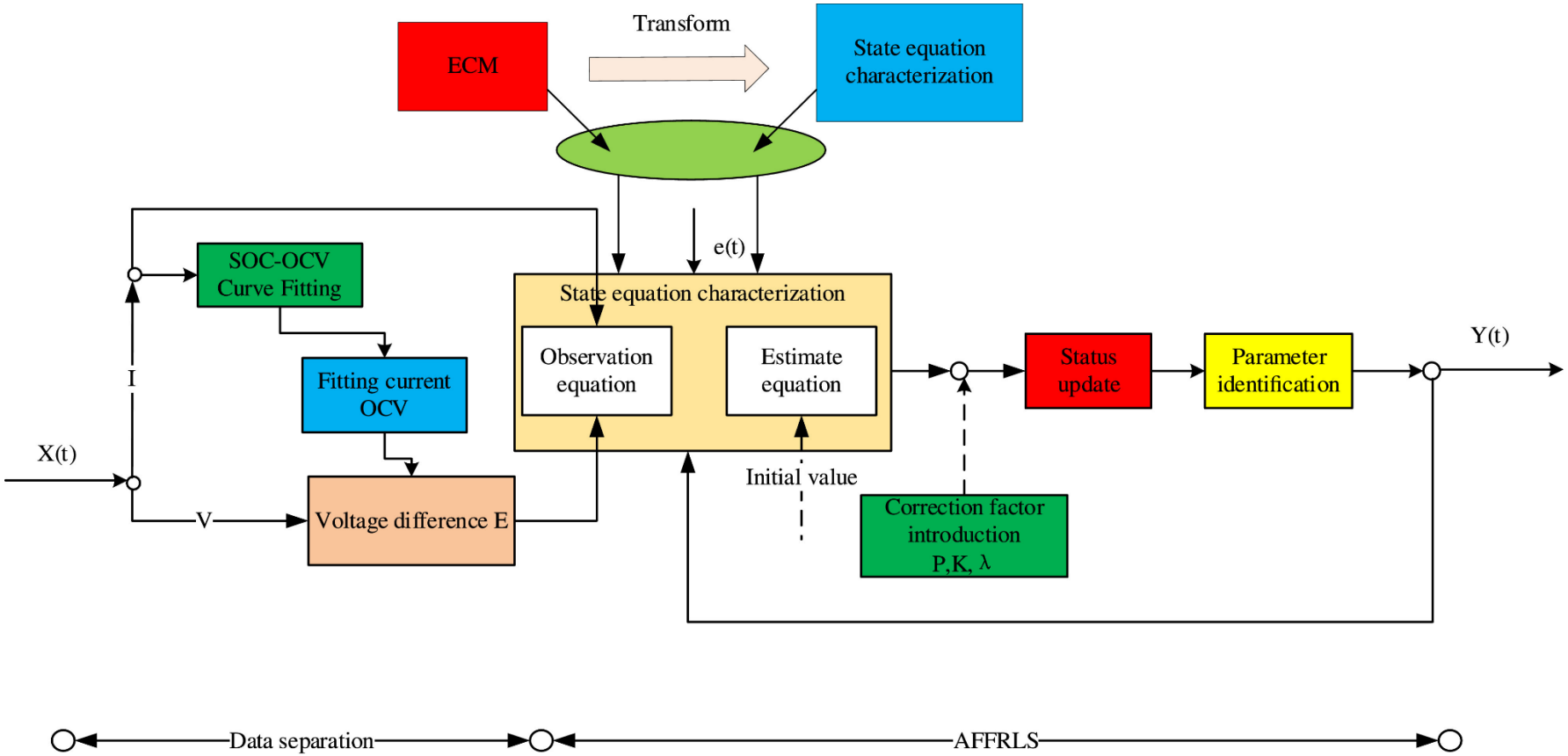

Fig. 2. The flow chart of AFFRLS algorithm for lithium-ion battery with pre-data processing

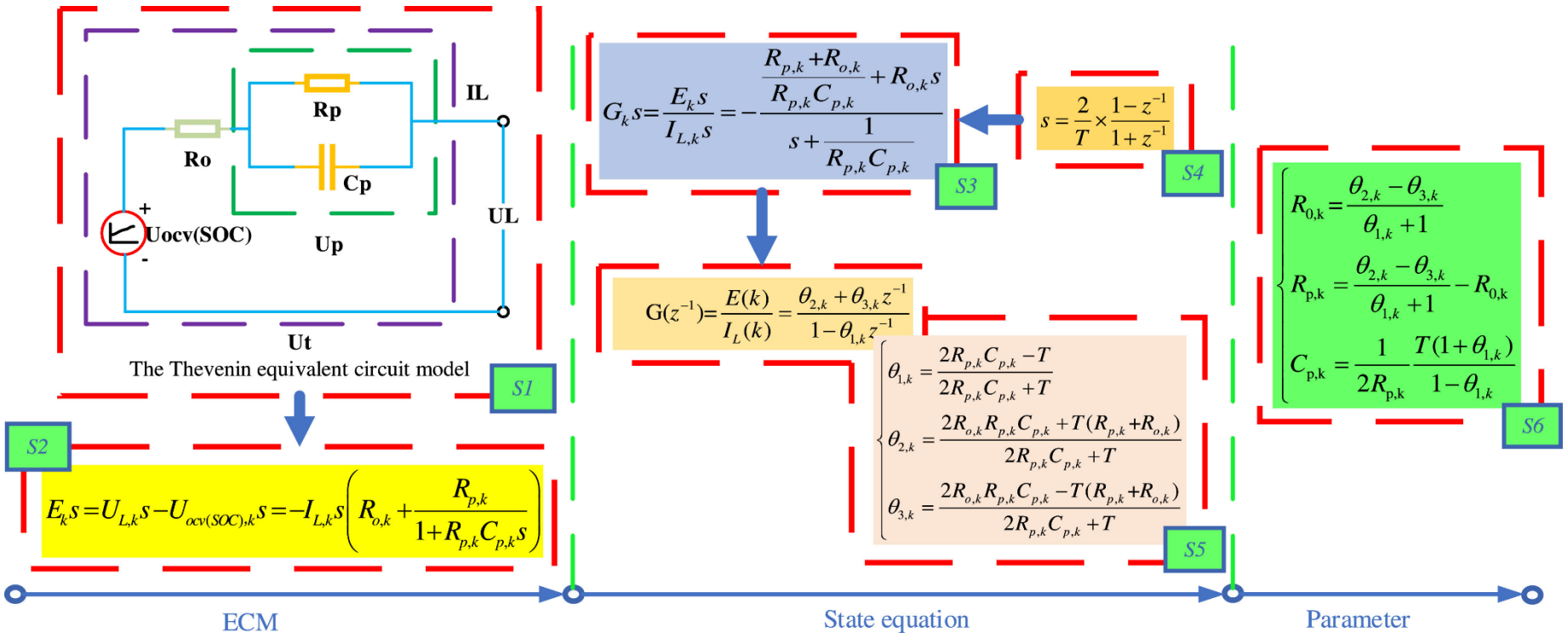

Fig. 3. The flowchart of the model's least squares form

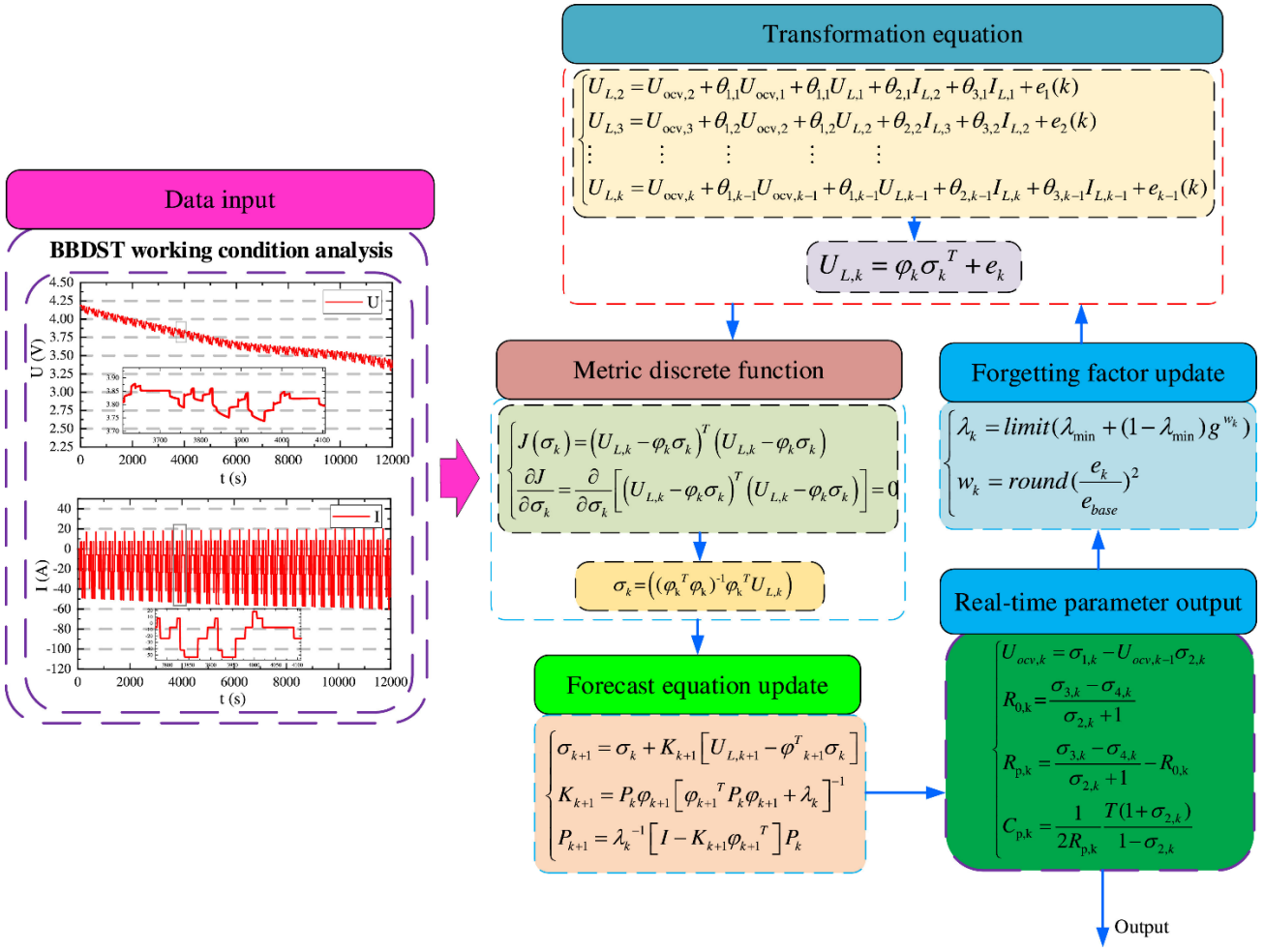

Fig. 4. The flow chart of the improved AFFRLS algorithm

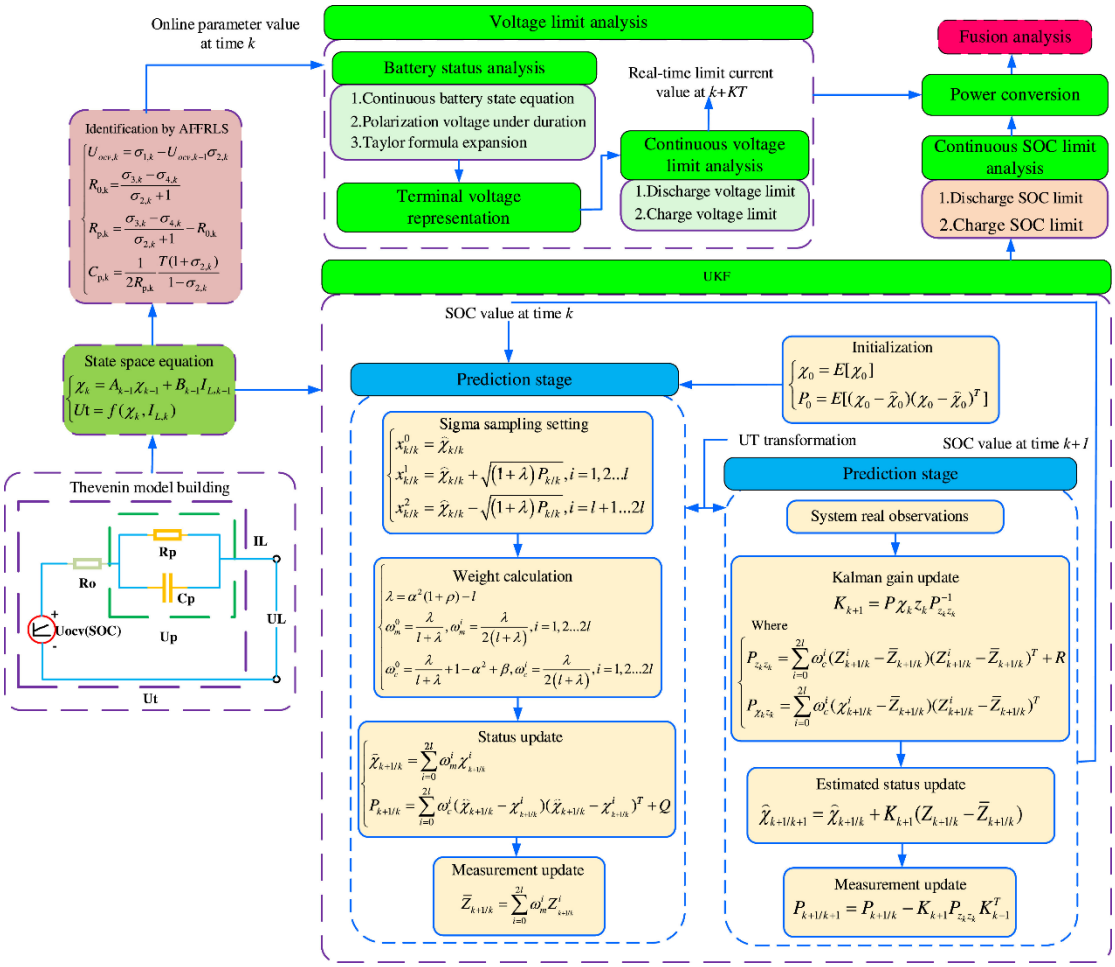

Fig. 5. The fusion estimation model under the limits of voltage and SOC

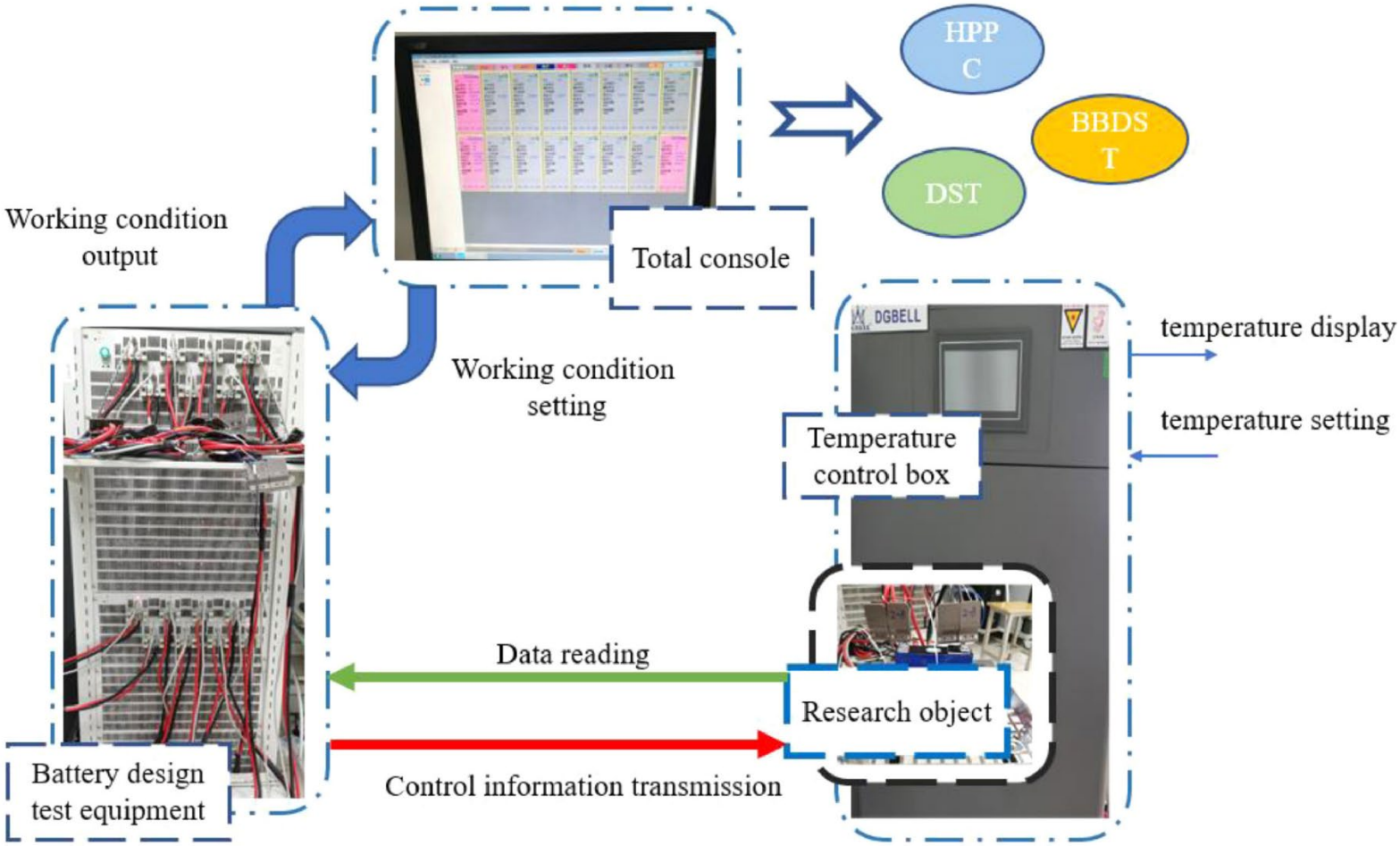

Fig. 6. The experimental data test flow of the research object

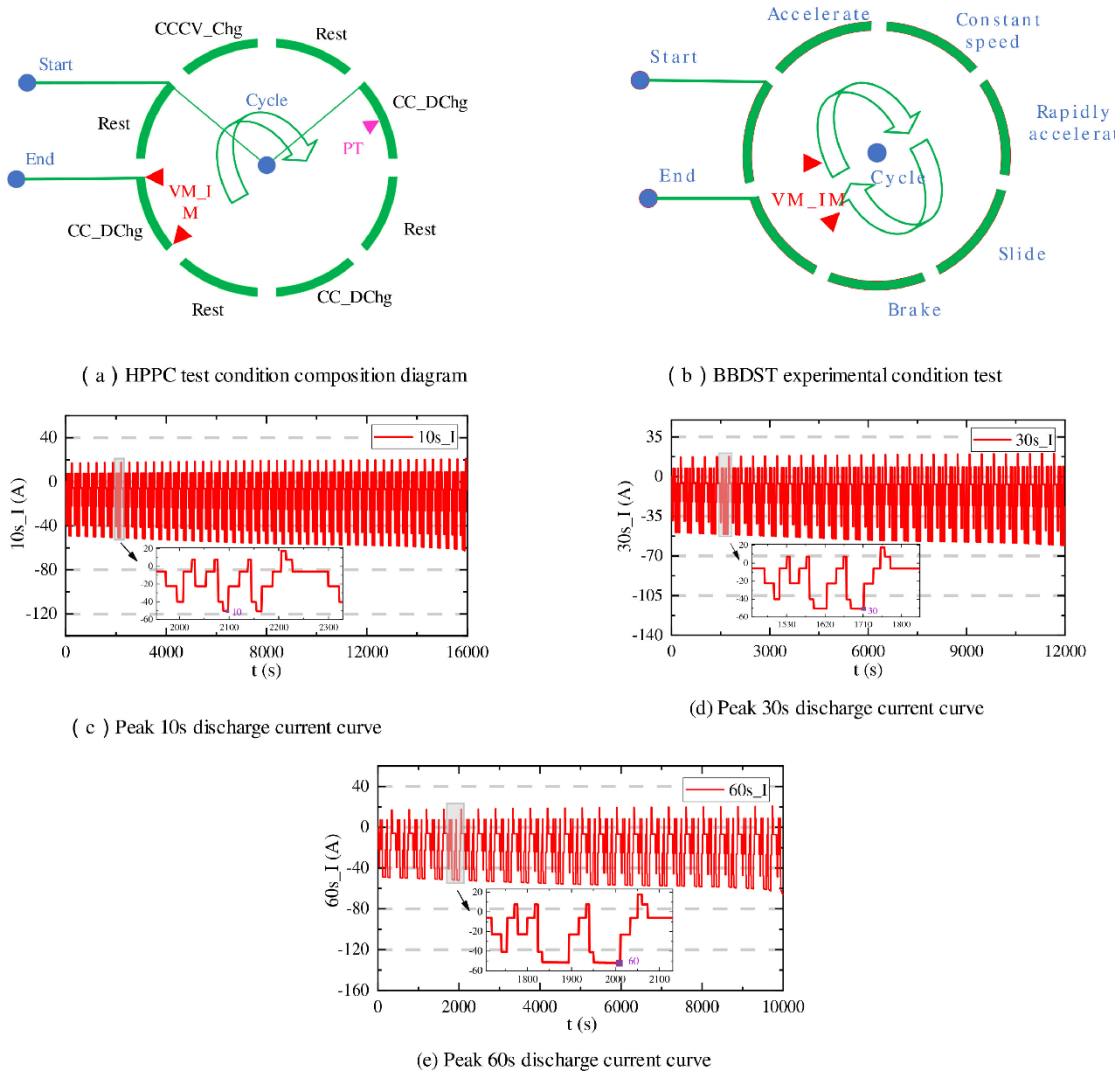

Fig. 7. The experimental data test flow of the research object

(a)HPPC test condition composition diagram

(b)BBDST experimental condition test

(c) Peak 10s discharge current curve

(d) Peak 30s discharge current curve

(e) Peak 60s discharge current curve

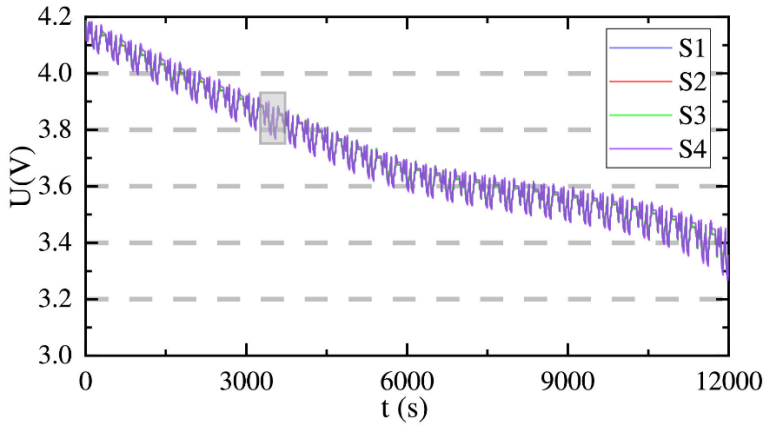

(a) Voltage error curve of lithium-ion battery

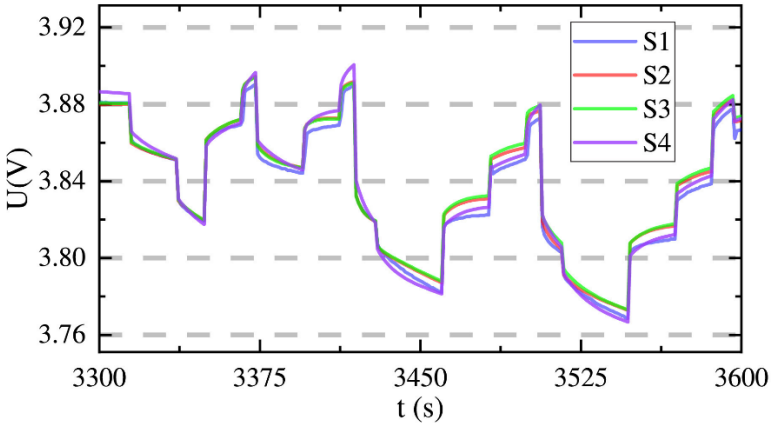

(b) Partially enlarged picture of voltage

Fig. 8. The voltage simulation error and its partial amplification error diagram

(a)Voltage error curve of lithium-ion battery (b) Partially enlarged picture of voltage

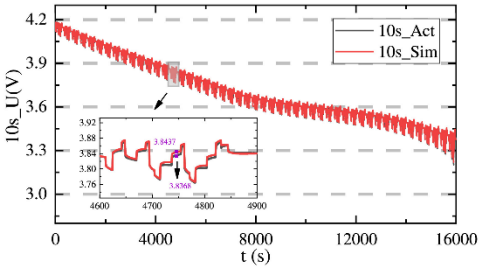

(a) On-line identification of voltage analysis curve at 10s peak discharge

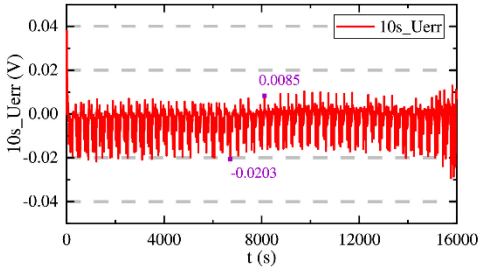

(b) On-line identification of voltage error curve at 10s peak discharge

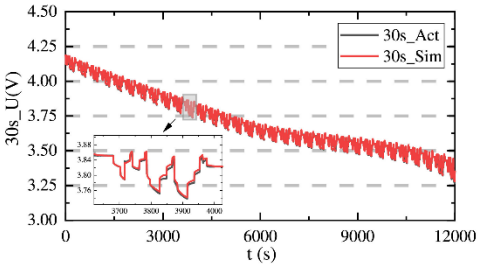

(c) On-line identification of voltage analysis curve at 30s peak discharge

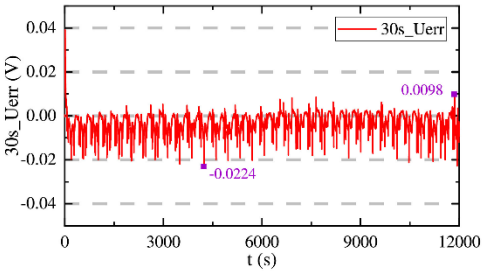

(d) On-line identification of voltage error curve at 30s peak discharge

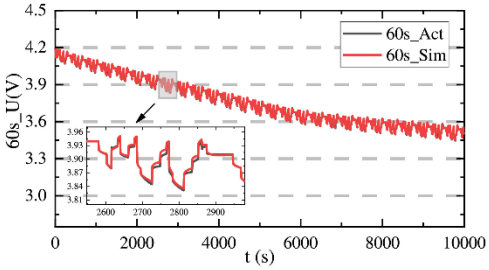

(e) On-line identification of voltage analysis curve at 60s peak discharge

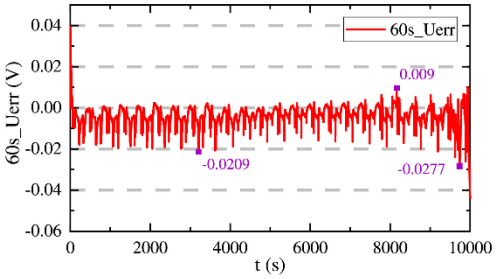

(f) On-line identification of voltage error curve at 60s peak discharge

Fig. 9. BBDST conditions under different continuous excitation and voltage errors curve

(a) On-line identification of voltage analysis curve at 10s peak discharge

(b) On-line identification of voltage error curve at 10s peak discharge

(c) On-line identification of voltage analysis curve at 30s peak discharge

(d) On-line identification of voltage error curve at 30s peak discharge

(e) On-line identification of voltage analysis curve at 60s peak discharge

(f) On-line identification of voltage error curve at 60s peak discharge

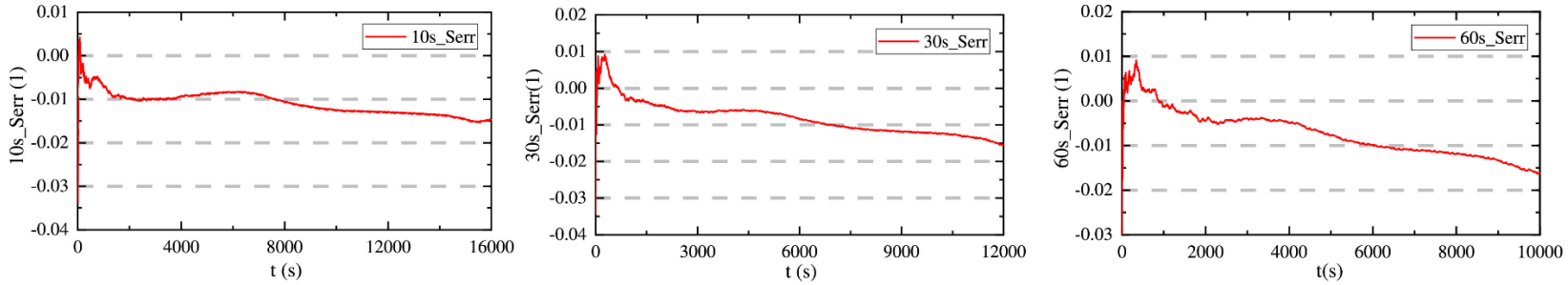

(a) SOC estimation error under 10s peak (b) SOC estimation error under 30s peak (c) SOC estimation error under 60s peak

Fig. 10. SOC estimation curve based on UKF under different continuous excitation

(a) SOC estimation error under 10s peak
(b) SOC estimation error under 30s peak
(c) SOC estimation error under 60s peak

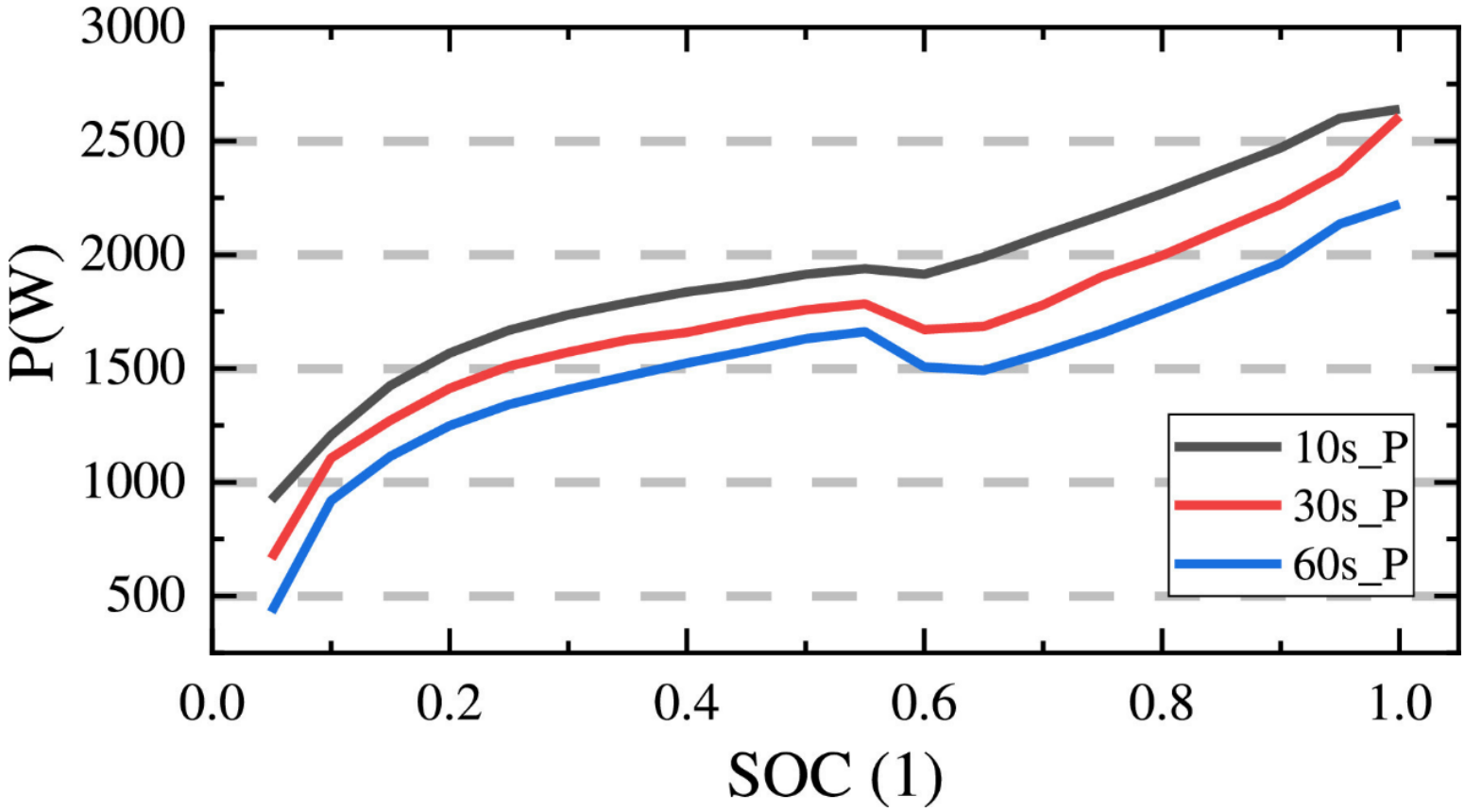

Fig. 11. Power curve under different discharge continuous excitation

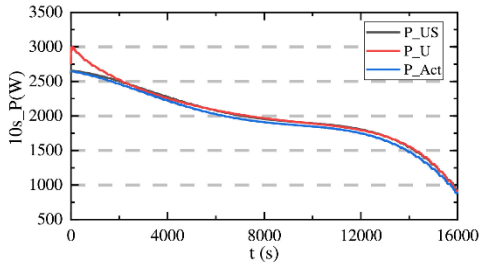

(a) SOP estimation curve based fusion model at 10s peak discharge

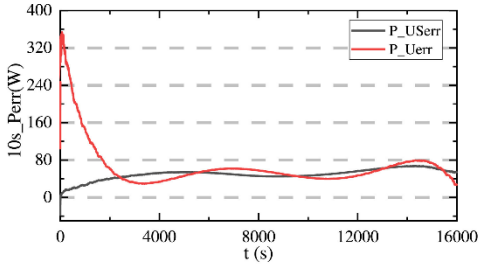

(b) SOP error curve at 10s peak discharge

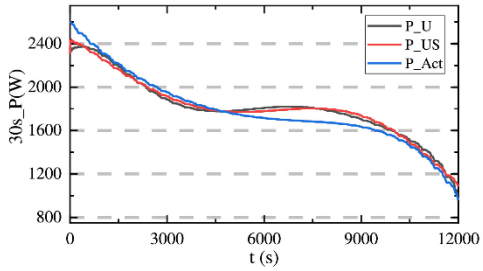

(c) SOP estimation curve based fusion model at 30s peak discharge

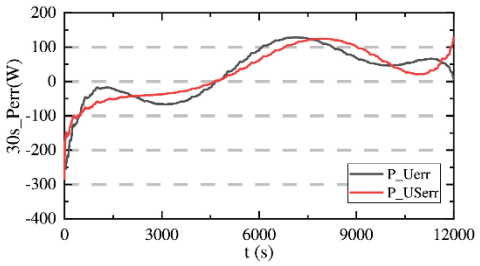

(d) SOP error curve at 30s peak discharge

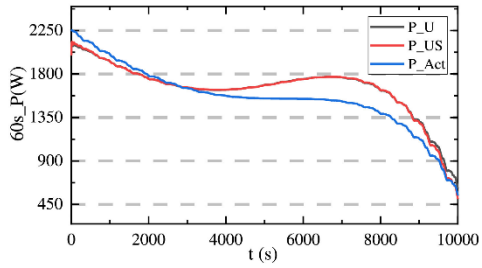

(e) SOP estimation curve based fusion model at 60s peak discharge

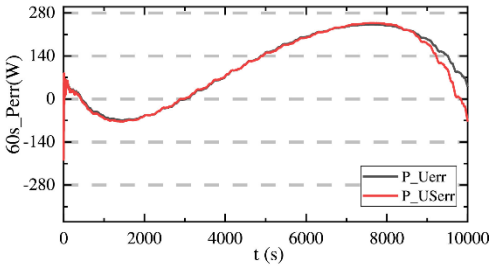

(f) SOP error curve at 60s peak discharge

Fig. 12. SOP estimation curve based on fusion model under different continuous excitation

(a) SOP estimation curve based fusion model at 10s peak discharge

(b) SOP error curve at 10s peak discharge

(c) SOP estimation curve based fusion model at 30s peak discharge

(d) SOP error curve at 30s peak discharge

(e) SOP estimation curve based fusion model at 60s peak discharge

(f) SOP error curve at 60s peak discharge

Table 1. Performance evaluation index of different algorithms

Algrithm	Performance		
	Mean squared error	Mean absolute error	Root mean squard error
AFFRLS with pre-data processing	0.0049	3.9464e-5	0.0063
Improved FRLS	0.0034	2.0602e-5	0.0045
Improved AFFRLS	0.0025	1.0908e-5	0.0033

Table 2. Full state performance estimation

Time	Performance	Error observation			
		U	SOC	P_U	P_US
10s	MAE	0.002	0.0092	65.4179	49.0931
	MSE	1.75e-05	9.27e-05	7.05e+03	3.03e+03
	RMSE	0.0042	0.0096	83.9513	55.0342
30s	MAE	0.0025	0.0082	65.3559	60.8035
	MSE	2.07e-05	7.97e-05	6.05e+03	5.89e+03
	RMSE	0.0045	0.0089	77.7608	76.9086
60s	MAE	0.0032	0.0075	133.2087	128.8349
	MSE	3.02e-05	7.29e-05	2.56e+04	2.51e+04
	RMSE	0.0055	0.0085	159.8933	158.4401